https://doi.org/10.31925/farmacia.2022.2.21 **ORIGINAL ARTICLE**

DESIGN, SYNTHESIS, BIOLOGICAL EVALUATION AND MOLECULAR DOCKING OF PYRROLE-BASED COMPOUNDS AS ANTIOXIDANT AND MAO-B INHIBITORY AGENTS

EMILIO MATEEV [1]*, BORISLAV ANGELOV [2], MAGDALENA KONDEVA-BURDINA [2], IVA VALKOVA [3], MAYA GEORGIEVA [1], ALEXANDER ZLATKOV [1]

[1]*Department of Pharmaceutical Chemistry, Faculty of Pharmacy, Medical University – Sofia, Bulgaria*
[2]*Department of Pharmacology, Pharmacotherapy and Toxicology, Faculty of Pharmacy, Medical University – Sofia, Bulgaria*
[3]*Department of Chemistry, Faculty of Pharmacy, Medical University – Sofia, Bulgaria*

**corresponding author: e.mateev@pharmfac.mu-sofia.bg*

Manuscript received: November 2021

Abstract

Alzheimer's disease (AD) is the most widespread neurodegenerative disorder with a significant impact on health systems. Considering the lack of efficient treatment, compounds with multi-target activities are usually designed as promising options to fill the evident gap. In this study, two novel N-pyrrolyl carboxylic acids (**4a** and **5a**) and eight corresponding amide derivatives (**4a1-4a3** and **5a1-5a5**) were synthesized and fully elucidated by ^{1}H NMR, FT-IR and HRMS (high resolution mass spectrometry). All reported compounds were assessed for their radical (DPPH and $ABTS^{+\bullet}$) scavenging properties and MAO-B blocking potential. The results indicated that compound **5a2** could serve as a prominent lead compound for a future optimization as a MAO-B inhibitor. In addition, the DPPH and $ABTS^{+\bullet}$ assays demonstrated significant antioxidant capacity. A possible binding conformation of **5a2** in the active site of MAO-B was also identified through molecular docking simulations. The analysis of the major interactions indicated the establishment of several unfavourable steric clashes. Thus, reducing the size of the core structure could drastically increase the MAO-B antagonizing potency of the pyrrole-based compounds.

Rezumat

Boala Alzheimer (AD), este cea mai răspândită tulburare neurodegenerativă cu un impact semnificativ asupra sistemelor de sănătate. De aceea compușii cu activitate multi-țintă sunt de obicei cercetați ca opțiuni terapeutice promițătoare. În acest studiu, doi noi acizi N-pirolil carboxilici (**4a** și **5a**) și opt derivați amidici (**4a1-4a3** și **5a1-5a5**) au fost sintetizați și analizați prin ^{1}H RMN, FT-IR și MS. Toți compușii au fost evaluați prin testele DPPH și $ABTS^{+\bullet}$ precum și pentru potențialul inhibitor MAO-B. Rezultatele au indicat că **5a2** ar putea servi drept inhibitor MAO-B eficient. În plus, testele DPPH și $ABTS^{+\bullet}$ au demonstrat capacitatea antioxidantă semnificativă. O posibilă conformație de legare a **5a2** în situsul activ al MAO-B a fost, de asemenea, identificată prin simulări de andocare moleculară. Analiza interacțiunilor majore a indicat stabilirea mai multor ciocniri sterice nefavorabile. Astfel, reducerea dimensiunii structurale a nucleului ar putea crește capacitatea de antagonizare a MAO-B a compușilor pirolici.

Keywords: MAO-B inhibitors, pyrrole, antioxidants, molecular docking

Introduction

Alzheimer's disease (AD) is a persistent illness, which causes personality changes, progressive deprivation of neuronal functionalities and further cognitive impairments [13]. The significant increase of patients suffering from the latter neurodegenerative disease [14], together with the uncertainty of the efficacy of the current therapy [10] has enhanced the interest in design and synthesis of novel anti-AD drugs.

Considering the complex pathogenesis of AD, the search of novel multi targeting molecules is a prominent option to slow the progression of the disease [18, 27]. Enzymes such as, acetylcholine (AChE), butyrylcholine (BuChE), Beta-secretase 1 (BACE1), Monoamine oxidase B (MAO-B) as well as Nicotinamide adenine dinucleotide phosphate oxidase (NADPH oxidase) are well established in the progression of AD. The former enzyme – NADPH oxidase, leads to the generation of reactive oxygen species (ROS) and thus, oxidative stress (OS), which has been associated with a cascade of inflammatory and degenerative pathologies. The role of oxidative stress in the progression of AD has been confirmed by numerous researchers [6, 25]. Therefore, the utilization of antioxidants in the treatment of AD could be determined as one of the most prominent therapeutic approaches [19].

Monoamine oxidases are enzymes involved in the termination of numerous essential monoamines, such as dopamine, serotonin, tyramine, melatonin and nor-epinephrine [7]. There are two reported isoforms – MAO-A and MAO-B, comprising around 70% identical amino acid sequences. From the two described isoforms, MAO-B predominates in the human brain and it is a

feasible target in the treatment of neurodegenerative diseases. That assumption is strongly affirmed after the approval of selegiline and rasagiline as effective drugs in the therapeutic scheme in Parkinson's disease [26]. In addition, the elevated levels of MAO-B in astrocytes and pyramidal neurons have been observed in patients with AD by Schedin-Weiss *et al*. [24]. Hence, compounds with MAO-B antagonizing activity could be considered as potential molecules against AD. However, several clinical trials have revealed poor results after utilizing selegiline in the treatment of AD [23], which demonstrates the requirement for novel effective MAO-B inhibitors.

Despite the broad pharmacological profile of the pyrrole moiety, there is a lack of research papers considering the latter motif as antioxidant or MAO-B inhibitor. In addition, the role of the amide moiety for the occurring antioxidant properties is evident [3, 22]. The aforementioned data led to the aim of the current paper, which was to synthesize novel pyrrole-based MAO-B inhibitors with amide moieties and to test *in vitro* the antioxidant capacities and MAO-B blocking activities. As a final stage of this work, virtual examinations of the major interactions between the ligands and the active site of MAO-B were carried out.

Materials and Methods

Chemistry

Available reactants and solvents were obtained from commercial suppliers and used without further purification, unless otherwise specified. Thin layer chromatography (TLC) was utilized for the monitoring of the reactions. The TLC characteristics of the products were measured on aluminium sheets of silica gel 60 F254, Merck 1.05554 at ambient temperature, employing a mobile phase of chloroform:ethanol = 10:1. The melting points were determined using Kruss M5000. UV/Visible scanning was carried out with Jenway 6715 Spectrophotometer. IR spectra within 4000 - 400 cm^{-1} range were recorded on a Nicolet iS10 FT-IR spectrometer using ATR technique with Smart iTR adapter (Thermo Fisher Scientific, USA). ^1H spectra was registered on Bruker Avance II+ 600 (Biospin GmbH, Rheinstetten, Germany) as δ (ppm) relative to TMS as internal standard, and the coupling constants (*J*) are expressed in hertz (Hz). Chemical shifts (δ) were stated in parts per million (ppm) relative to DMSO-d_6 (solvent). The mass spectra were acquired with a 6410 Agilent LCMS triple quadrupole mass spectrometer (LC-MS) with an electrospray ionization (ESI) interface (Agilent Technologies, USA).

The utilized synthetic path is provided in Figure 1.

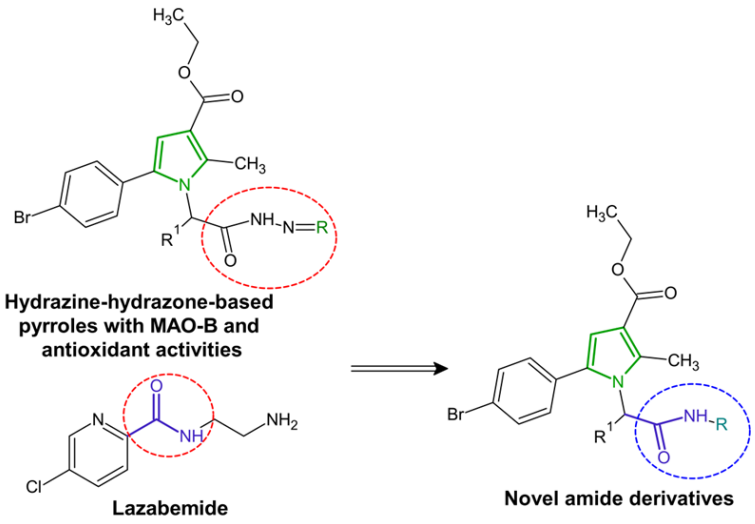

Figure 1.
The design of novel amide derivatives

*General procedure for synthesis of 1,4-dicarbonyl compounds (***3***)*

The dicarbonyl compound (**3**) was obtained according to a recently reported procedure by Bijev *et al*. [4].

General procedure for the synthesis of N-pyrrolyl-carboxylic acids (**4a, 5a**)

0.1 mol ethyl 2-acetyl-4-(4-bromophenyl)-4-oxo-butanoate (**3**) and 1.2 mol of valine (**a**) or isoleucine (**b**), were dissolved in 60 mL of glacial acetic acid. The mixture was heated and stirred for 4 - 5 h. Subsequently, the mixture was cooled at room temperature and poured into ice water. The precipitate was dissolved in CH_3Cl, worked up with 5% NaOH and 5% HCl and washed several times with water. The final product was dried and re-crystallized by appropriate solvent.

*General procedure for the synthesis of N-pyrrole carboxamides (***4a-4a3; 5a-5a5***)*

To a solution of N-pyrrolylcarboxylic acids **(4a, 5a)** (0.1 mmol), 4-N,N-dimethylaminopyridine (DMAP) (0.1 mmol) and corresponding amines in CH_2Cl_2 (3 mL) at 0°C, was added dicyclohexylcarbodiimide (DCC) (0.12 mmol) dissolved in 1 mL CH_2Cl_2. The reactions

were refluxed while stirring at room temperature for 11.5 - 30 h and monitored by TLC using CH_3Cl-EtOH (10:1). The DCU was filtered and the DCM was removed by evaporation under reduced pressure. The obtained compounds were acid-base extracted, followed by drying and re-crystallization of the final product with ethanol/water.

2-[5-(4-bromophenyl)-3-(ethoxycarbonyl)-2-methyl-1H-pyrrol-1-yl]-3-methylbutanoic acid (**4a**): Colourless crystals; yield 88%; m.p.: 105.2 - 105.6; IR spectrum (ν, cm^{-1}): 3300 (O-H), 1720, 1695 (C=O), 780, 750 cm^{-1} (*p*-C_6H_4); 1580 (C=C) cm^{-1}; ^{1}H NMR (DMSO-*d*6, 600 MHz)**:** δ 10.14 (d, 1H, *J* = 10.7 Hz, CHCOOH), 7.55 - 7.78 (m, 4H, C_6H_4), 6.78 (s, 1H, H-4), 5.40 (br, s, 1H, COOH), 4.29 (q, 2H, *J* = 7.1 Hz, CH_3CH_2), 2.00 [m, 4H, CH_3-2 + CH (isopropyl)], 1.30 (t, 3H, *J* = 7.1 Hz, CH_3CH_2), 0.93 [d, 3H, *J* = 6.3 Hz, CH_3 (isopropyl)], 0.93 [d, 3H, *J* = 6.8 Hz, CH_3 (isopropyl)]; MS: *m/z* = 408.286.

Ethyl 5-(4-bromophenyl)-1-(1-((4-chlorophenyl)-amino)-3-methyl-1-oxobutan-2-yl)-2-methyl-1H-pyrrole-3-carboxylate (**4a1**): Colourless crystals; yield 57%; m.p.: 169.1 - 169.3; IR spectrum (ν, cm^{-1}): 3350 - 3310 cm^{-1} (NH), 1705 cm^{-1} (C=O), 1580 cm^{-1} (C=C), 830, 750 cm^{-1} (*p*-C_6H_4); ^{1}H NMR (DMSO-*d*6, 600 MHz)**:** δ 10.02 (s, 1H, *J* = 7.00 Hz, NH), 7.55 - 7.78 (m, 4H, C_6H_4), 6.78 (s, 1H, H-4), 4.29 (q, 2H, *J* = 7.1 Hz, CH_3CH_2), 2.00 [m, 4H, CH_3-2 + CH (isopropyl)], 1.30 (t, 3H, *J* = 7.1 Hz, CH_3CH_2), 0.93 [d, 3H, *J* = 6.3 Hz, CH_3 (isopropyl)]; MS: *m/z* = 517.846.

Ethyl 5-(4-bromophenyl)-1-(1-((4-bromophenyl)-amino)-3-methyl-1-oxobutan-2-yl)-2-methyl-1H-pyrrole-3-carboxylate (**4a2**): Colourless crystals; yield 60%; m.p.: 165.6 - 165.8; IR spectrum (ν, cm^{-1}): 3350-3310 cm^{-1} (NH); 1705 cm^{-1} (C=O), 1580 cm^{-1} (C=C), 830, 750 cm^{-1} (*p*-C_6H_4); ^{1}H NMR (DMSO-*d*6, 600 MHz)**:** δ 10.02 (s, 1H, *J* = 7.00 Hz, NH), 7.55 - 7.78 (m, 4H, C_6H_4), 6.78 (s, 1H, H-4), 4.29 (q, 2H, *J* = 7.1 Hz, CH_3CH_2), 2.00 [m, 4H, CH (isopropyl)], 1.30 (t, 3H, *J* = 7.1 Hz, CH_3CH_2), 0.93 [d, 3H, *J* = 6.3 Hz, CH_3 (isopropyl)], 7.52 (m, 4H, C_6H_4); MS: *m/z* = 562.295.

Ethyl 5-(4-bromophenyl)-1-(1-((4-methoxyphenyl)-amino)-3-methyl-1-oxobutan-2-yl)-2-methyl-1H-pyrrole-3-carboxylate (**4a3**): Colourless crystals; yield 48%; m.p.: 171.1 - 171.9; IR spectrum (ν, cm^{-1}): 3120 - 3240 cm^{-1} (NH); 1695 cm^{-1} (C=O), 1530 cm^{-1} (C=C), 820, 710 cm^{-1} (*p*-C_6H_4); ^{1}H NMR (DMSO-*d*6, 600 MHz): δ 10.02 (s, 1H, *J* = 7.00 Hz, NH), 7.55 - 7.78 (m, 4H, C_6H_4), 7.45 - 6.86 (m, 4H, C_6H_4); 6.78 (s, 1H, H-4), 4.29 (q, 2H, *J* = 7.1 Hz, CH_3CH_2), 3.81 (s, 3H, OCH_3), 2.00 [m, 4H, CH (isopropyl)], 1.30 (t, 3H, *J* = 7.1 Hz, CH_3CH_2), 0.93 [d, 3H, *J* = 6.3 Hz, CH_3 (isopropyl)]; MS: *m/z* = 513.427.

2-(5-(4-bromophenyl)-3-(ethoxycarbonyl)-2-methyl-1H-pyrrol-1-yl)-3-methylpentanoic acid (**5a**): Reddish crystals, yield 82%; m.p.: 117.1 - 171.2; IR spectrum (ν, cm^{-1}): 3300 cm^{-1} (O-H), 1710 cm^{-1} (C=O), 1570 cm^{-1} (C=C) cm^{-1}, 760 - 730 cm^{-1} (*p*-C_6H_4); ^{1}H NMR (DMSO-*d*6, 600 MHz): δ 12.22 (s, 1H, COOH), 7.55 - 7.78 (m, 4H, C_6H_4), 6.78 (s, 1H, H-4), 4.29 (q, 2H, *J* = 7.1 Hz, CH_3CH_2), 1.8 (m, 1H, $CHCH_3$), 1.55 (m, 2H, CH_2CH_3), 1.30 (t, 3H, CH_3CH_2), 0.93 (d, 3H, *J* = 6.3 Hz, $CHCH_3$); MS: *m/z* = 422,122.

Ethyl 5-(4-bromophenyl)-1-(1-(4-(4-chlorobenzyl)-piperazin-1-yl)-3-methyl-1-oxopentan-2-yl)-2-methyl-1H-pyrrole-3-carboxylate (**5a1**): Red crystals, yield 41%; m.p.: 184.1 - 185; IR spectrum (ν, cm^{-1}): 3050 - 2870 cm^{-1} (NH); 1695 cm^{-1} (C=O), 1530 - 1410 (C=C), 820, 710 cm^{-1} (*p*-C_6H_4); ^{1}H NMR (DMSO-*d*6, 600 MHz): δ 7.55 - 7.78 (m, 4H, C_6H_4), 7.32 - 7.39 (m, 4H, C_6H_4), 6.78 (s, 1H, H-4), 4.29 (q, 2H, *J* = 7.1 Hz, CH_3CH_2), 3.66 (s, 2H, CH_2), 2.48 - 3.30 (m, 8H, $N_2C_4H_8$), 1.8 (m, 1H, $CHCH_3$), 1.55 (m, 2H, CH_2CH_3), 1.30 (t, 3H, CH_3CH_2), 0.93 (d, 3H, *J* = 6.3 Hz, $CHCH_3$), MS: *m/z* = 615.017.

Ethyl 5-(4-bromophenyl)-1-(1-(4-(4-bromophenyl)-piperazin-1-yl)-3-methyl-1-oxopentan-2-yl)-2-methyl-1H-pyrrole-3-carboxylate (**5a2**): Yellow crystals, yield 45%; m.p.:168 - 168.7; IR spectrum (ν, cm^{-1}): 3230 - 2920 cm^{-1} (NH); 1715 cm^{-1} (C=O), 1540 - 1450 cm^{-1} (C=C); ^{1}H NMR (DMSO-*d*6, 600 MHz): δ 7.55 - 7.78 (m, 4H, C_6H_4), 7.17 - 7.85 (m, 4H, C_6H_4), 6.78 (s, 1H, H-4), 4.29 (q, 2H, *J* = 7.1 Hz, CH_3CH_2), 3.66 (s, 2H, CH_2), 2.48 - 3.30 (m, 8H, $C_4H_8N_2$), 1.8 (m, 1H, $CHCH_3$), 1.55 (m, 2H, CH_2CH_3), 1.30 (t, 3H, CH_3CH_2), 0.93 (d, 3H, *J* = 6.3 Hz, $CHCH_3$); MS: *m/z* = 645.423.

Ethyl 5-(4-bromophenyl)-2-methyl-1-(3-methyl-1-(naphthalen-1-ylamino)-1-oxopentan-2-yl)-1H-pyrrole-3-carboxylate (**5a3**): Gray crystals, yield 55%; m.p.: 174.2 - 174.9; IR spectrum (ν, cm^{-1}): 3200 - 3000 cm^{-1} (NH); 1730 cm^{-1} (C=O), 1520 - 1440 cm^{-1} (C=C); ^{1}H NMR (DMSO-*d*6, 600 MHz): δ 10.22 (s, 1H, NH), 8.29 - 7.68 (m, $C_{10}H_9N$), 7.55 - 7.78 (m, 4H, C_6H_4), 6.78 (s, 1H, H-4), 4.29 (q, 2H, *J* = 7.1 Hz, CH_3CH_2), 1.8 (m, 1H, $CHCH_3$), 1.55 (m, 2H, CH_2CH_3), 1.30 (t, 3H, CH_3CH_2), 0.93 (d, 3H, *J* = 6.3 Hz, $CHCH_3$); MS: *m/z* = 547.474.

Ethyl 5-(4-bromophenyl)-1-(1-((2,4-dinitrophenyl)-amino)-3-methyl-1-oxopentan-2-yl)-2-methyl-1H-pyrrole-3-carboxylate (**5a4**): Yellow crystals, yield 27%; m.p.: 189.4 - 189.8; IR spectrum (ν, cm^{-1}): 3450 - 3560 cm^{-1} (NH); 1695 cm^{-1} (C=O), 1490 - 1510 cm^{-1} (C=C); ^{1}H NMR (DMSO-*d*6, 600 MHz): δ 10.02 (s, 1H, NH), 8.07 - 8.77 (m, 3H), 7.55 - 7.78 (m, 4H, C_6H_4), 6.78 (s, 1H, H-4), 4.29 (q, 2H, *J* = 7.1 Hz, CH_3CH_2), 1.55 (m, 2H, CH_2CH_3), 1.82 (m, 1H, $CHCH_3$), 1.30 (t, 3H, CH_3CH_2), 0.93 (d, 3H, *J* = 6.3 Hz, $CHCH_3$); MS: *m/z* = 587.423.

Ethyl 5-(4-bromophenyl)-2-methyl-1-(3-methyl-1-((2-methylquinolin-4-yl)amino)-1-oxopentan-2-yl)-1H-pyrrole-3-carboxylate (**5a5**): White crystals, yield 27%; m.p.: 189.4 - 189.8; IR spectrum (ν, cm^{-1}): 3000 - 3120 cm^{-1} (NH); 1700 cm^{-1} (C=O), 1540 - 1570 cm^{-1} (C=C); ^{1}H NMR (DMSO-*d*6, 600 MHz):

δ 9.92 (s, 1H, *J* = 7.00 Hz, NH), 7.55 - 7.78 (m, 4H, C_6H_4), 6.78 (s, 1H, H-4), 4.29 (q, 2H, *J* = 7.1 Hz, CH_3CH_2), 2.53 (s, 3H, CH_3), 1.82 (m, 1H, $CHCH_3$), 1.55 (m, 2H, CH_2CH_3), 1.30 (t, 3H, CH_3CH_2), 0.93 (d, 3H, *J* = 6.3 Hz, $CHCH_3$); MS: *m/z* = 562.491.

MAO-B

Monoamine oxidase activity assay of recombinant human MAO-B was performed using a fluorometric method by Amplex UltraRed reagent [2] with small modifications. Tyramine hydrochloride was used as substrate.

$ABTS^{+\bullet}$ Assay

In this study, the $ABTS^{+\bullet}$ antioxidant capacities of the compounds were measured according to a modified method of Arnao *et al*. [1]. The analyses were carried out in methanol at ambient temperature and the absorbance was measured at λ = 734 nm. The mother solution consisted of 7 mmol/L solution of $ABTS^{+\bullet}$ and 2.4 mmol/L solution of potassium per-sulphate, which were mixed and allowed to react for 14 h in dark at room temperature. The working solutions comprised 2 mL of the stock solution diluted in 50 mL of methanol with an absorbance of 0.302 ± 0.04 units at 517 nm. Different concentrations of the pyrrole derivatives were allowed to react with 1 mL of the $ABTS^{+\bullet}$ solution for 7 min with a subsequent absorbance determination. All of the determinations were carried out in triplicate. The capability of the pyrrole based compounds to neutralize the $ABTS^{+\bullet}$ radical was compared with that of Trolox and was calculated using the following equation (1):

$$ABTS_{scavengingactivity}\% = [(Abs_{control} - Abs_{sample}) / Abs_{control}] \times 100, \quad (1)$$

where $Abs_{control}$ is the absorbance of $ABTS^{+\bullet}$ radical in methanol and Abs_{sample} is the absorbance of DPPH radical solution mixed with sample.

DPPH Assay

DPPH (2,2- diphenyl-1-picrylhydrazyl) is a stable free-radical molecule frequently utilized for an anti-oxidant assays. A DPPH solution in methanol has an intense violet colour with UV absorption at 515 nm. In the presence of antioxidants or free radical species, the DPPH solution is decolourized and the inhibition capacities could be monitored by a decrease of the absorption. In the current study, the scavenging rate of DPPH radical was carried out by the widely employed classical protocol of Brand-Williams *et al*. [17]. Briefly, 5 different concentrations ranging from 1 - 0.125 µM of each amide in methanol were obtained (1 mL), followed by the addition of 1 mL methanol solution of DPPH (1 mmol/L). Each reaction mixture was vortex mixed and stored in the dark at ambient temperature for 30 min. The absorbance was measured at 517 nm using Jenway 6715 UV/Visible Scanning Spectro-photometer. Three measurements were conducted for each sample. The data demonstrated standard deviation below 5%. 6-Hydroxy-2,5,7,8- tetramethylchroman-2-carboxylic acid (Trolox) was used as a standard. The scavenged DPPH radicals were calculated in percent by equation (2):

$$DPPH_{scavenging\ activity} = [(Abs_{control} - Abs_{sample}) / Abs_{control}] \times 100, \quad (2)$$

where $Abs_{control}$ is the absorbance of DPPH radical in methanol and Abs_{sample} is the absorbance of DPPH radical solution mixed with sample.

Statistical analysis

The MAO-B IC_{50} values of the aforementioned compounds were calculated with GraphPad Prism Software. The results are expressed as a mean ± SD (n = 3). Values of $p < 0.05$ were considered statistically significant.

Molecular Docking

Docking simulations were performed with Glide (Schrödinger Release 2021-3: Glide, Schrödinger, LLC, New York, NY, 2021) on an AMD Ryzen 5 3600 6-core 3.6 GHz CPU, GeForce GTX 1060 3 GB GPU, 16 GB RAM installed memory and 64-bit Operating system Windows 10 Pro.

The crystal structure with PDB code **6FW0** comprising a bulky amide co-crystallized ligand was chosen for the current work. It was retrieved from the Protein Data Bank (PDB) [33] with a reliable resolution of 1.60 Å. The protein preparation module in Schrodinger [12] was utilized for the initial preparation of the receptor. Receptor Grid Generator in Maestro was used for determining the active grid space, which was cantered on the co-crystallized ligand.

The compounds were drawn in ChemDraw (Perkin-Elmer Informatics) and converted to the corresponding 3D structures with the LigPrep module in Maestro [28]. Utilising the latter, addition of hydrogen atoms, bond order assignment and energy minimization with OPLS3e force field were carried out.

The docking protocol was constructed out of all active waters (HOH814, HOH827, HOH834, HOH849, HOH853, HOH873, HOH899, HOH902, HOH908, HOH928 and HOH1077), 10 Å grid space and extra precision (XP) scoring of the obtained poses. The major interactions between compounds **5a2** and the active site the receptor were visualized employing Discovery Studio Visualizer (BIOVIA Dassault Systèmes, Pharmacopeia, Inc) and Maestro (Schrödinger Release 2021-3: Maestro, Schrödinger, LLC, New York, NY, 2021).

Prediction of ADME properties

To calculate the significant physicochemical and pharmacokinetic properties of the most prominent antioxidant and MAO-B antagonist in our dataset, ADME test was performed utilizing QikProp module in Schrodinger (Schrödinger Release 2021-2: QikProp, Schrödinger, LLC, New York, NY, 2021.). The simulation provides ranges based on the properties of 95% of the known drugs and also evaluates outliners based on the Lipinski's rule of five [11].

Results and Discussion

Design and synthesis of the pyrrole analogues

Previous studies have demonstrated that pyrrole-based hydrazones act as a promising MAO-B inhibitors and antioxidants [16]. In addition, several papers have described enhanced antioxidant capacities when an amide moiety was employed in the structures, with a particular attention given to the piperazine-based amides [17, 21]. Furthermore, the amide motif is present in several potent MAO-B inhibitors, such as safinamide and lazabemide [8, 32]. Considering the aforementioned observations, we designed and synthesized pyrrole analogues containing secondary amides, including substituted piperazines, with examination towards their antioxidant and MAO-B blocking activities (Figure 1). To explore whether chemically different moieties, such as benzyl, piperzyl, halogen based and others, have impact on the antioxidant and MAO-B activities, various amines were introduced into the processes of amide coupling reactions.

The N-pyrrolylcarboxylic acids were synthesized following the general Paal-Knorr approach with few modifications [30]. For the current work, the amino-acids valine and isoleucine were utilized for a condensation reaction with ethyl 2-acetyl-4-(4-bromo-phenyl)-4-oxobutanoate (Figure 2). The intermediate dicarbonyl molecule was produced by C-alkylation of the commercially available 2,4'-dibromoaceto-phenone and ethyl 3-oxobutanoate. The syntheses of the pyrrole carboxamides (**4a3**-**5a5**) were achieved *via* a DCC/DMAP coupling of N-pyrrolylcarboxylic acids with the corresponding amines, resulting in moderate yields of 27 - 60%.

The corresponding melting points, reaction times and yields for the employed amide structures are provided in Table I.

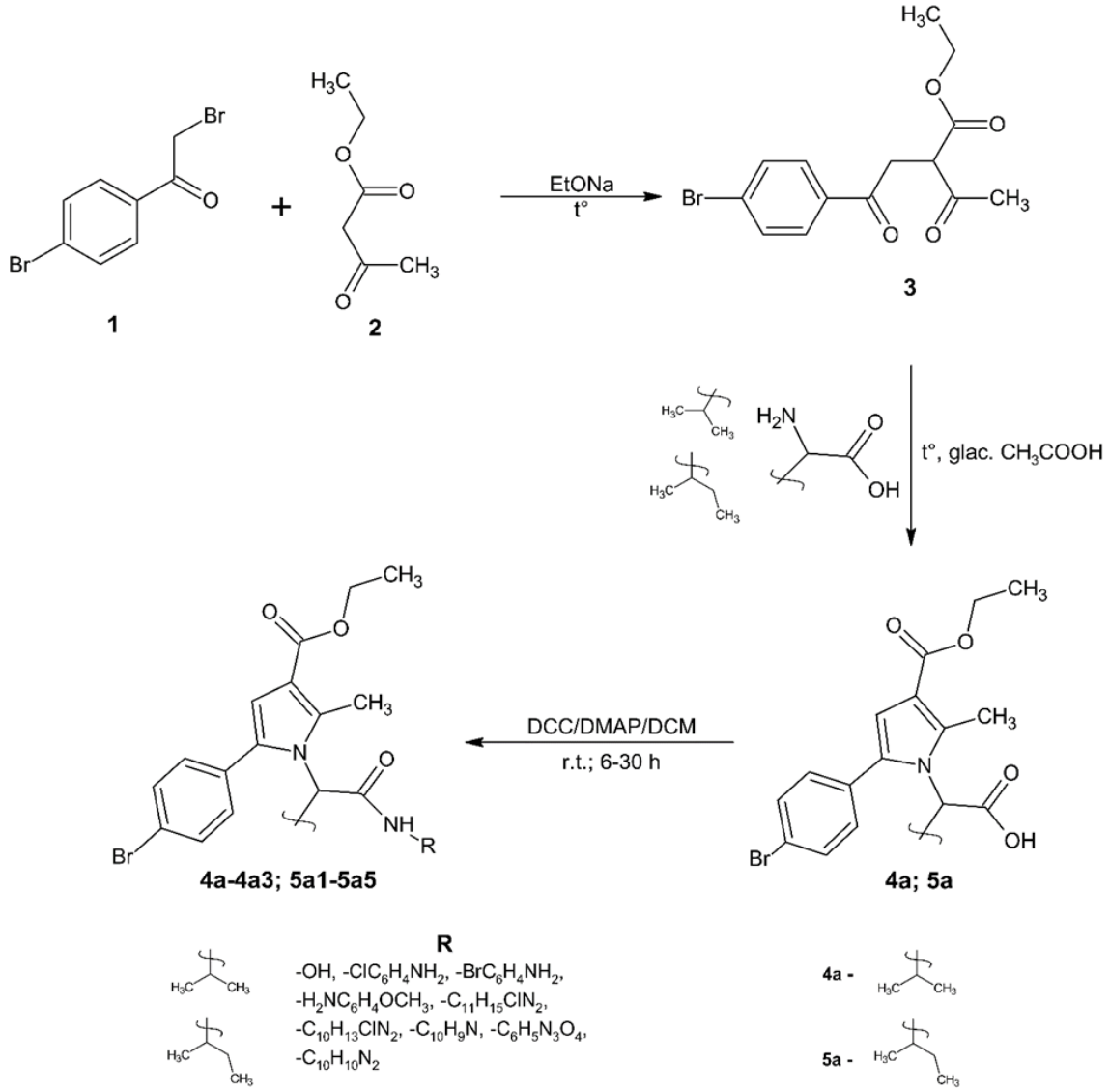

Figure 2.
Synthetic scheme of the target compounds

Table I

Substitutes, melting points, yields and reaction times of the novel amide derivatives

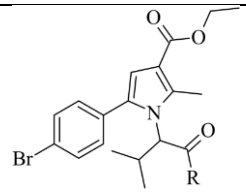

4a

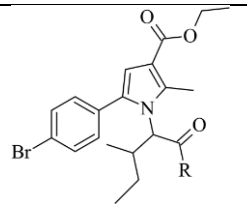

5a

Compound	R-fragment	M.P. (°C)	Reaction time (h)	Yield (%)
4a	—OH	105.2 - 105.6	6	88%
4a1	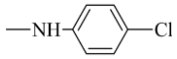	169.1 - 169.3	12	57%
4a2	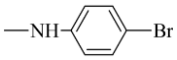	165.6 - 165.8	11.5	60%
4a3	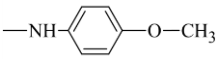	171.1 - 171.9	18	48%
5a	—OH	117.1 - 117.2	8.5	82%
5a1	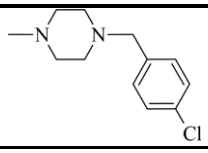	184.1 - 185	24	41%
5a2	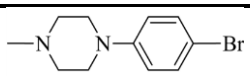	168 - 168.7	24	45%
5a3	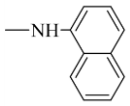	174.2 - 174.9	12	55%
5a4	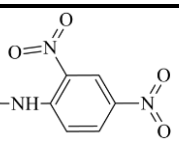	189.4 - 189.8	15	27%
5a5	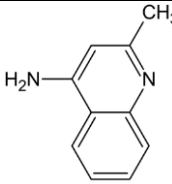	210.1 - 210.9	30	35%

Antioxidant activities

Two methods were applied in order to assess the antioxidant activities of the compounds – $ABTS^{+\bullet}$ and DPPH radical scavenging assays. Several advantages of $ABTS^{+\bullet}$ over DPPH, such as the ability to examine both hydrophobic and hydrophilic compounds, as well as to test bulky structures have been described elsewhere [9].

$ATBS^{+\bullet}$

During the $ABTS^{+\bullet}$ assay, the evaluated antioxidant neutralizes the $ABTS^{+\bullet}$ cation, which could be detected by the discolouration of the initial greenish colour of the solution. Variations of the absorbance levels at 734 nm are detectable. Lower absorbance indicates that a compound possess higher antioxidant capacity. The $ABTS^{+\bullet}$ antioxidant assay of the compounds is presented on Figure 3.

The obtained results pointed out that the condensed acids – **4a** and **5a**, demonstrate no relevant antioxidant activities. Moreover, a lack of $ABTS^{+\bullet}$ activity was detected for the newly synthesized amide derivatives of the acid **4a - 4a1-4a3** were examined. Interestingly, when the amino acid was altered to valine and the amide coupling was carried out with piperazine derivatives, significantly higher $ABTS^{+\bullet}$ scavenging activities were detected. Indeed, when compounds **5a1** and **5a2** were applied at 250 μM concentration, the latter demonstrated excellent antioxidant capacities of 99.87% and 81.28%, respectively. In addition, the 31 μM and 125 μM concentrations of comp. **5a1** displayed drastically higher $ABTS^{+\bullet}$ scavenging capacity compared to the standard Trolox. Weak $ABTS^{+\bullet}$ antioxidant capacities were demonstrated when 1-naphthylamine and 4-aminoquinaldine were presented into the

coupling reactions. Consequently, it may be concluded that the piperazine moiety heavily influenced the anti-radical scavenging abilities of the examined compounds.

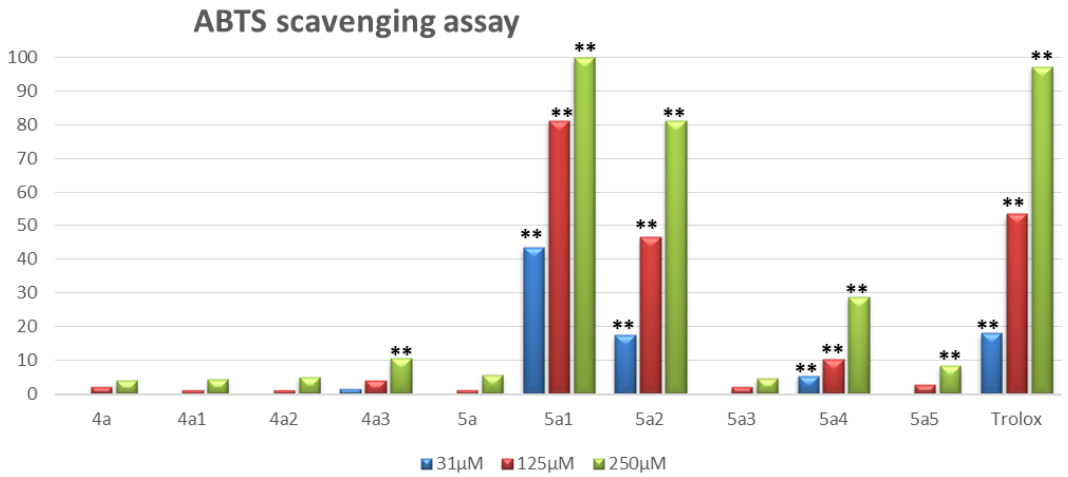

Figure 3.

ABTS$^{+\bullet}$ assay of the compounds at concentrations 31 to 250 µM

Standard deviation (SD) (n = 3). Significant difference *vs*. control: *p < 0.01; **p < 0.001

DPPH

The scavenging activity in 1,1-diphenyl-2-picryl-hydrazyl (DPPH) assay is attributed to the hydrogen donating ability of antioxidants with a subsequent decrease of the absorbance at 517 nm wavelength. Identical to the aforementioned ABTS$^{+\bullet}$ assay, the lower absorbance indicates for enhanced free radical scavenging activity.

The antioxidant effects of compounds **4a, 4a1-4a3** and **5a, 5a1-5a5** (at concentrations – 31 µM, 125 µM and 250 µM) were examined and the results were compared with these of Trolox used at the same concentrations and are presented on Figure 4.

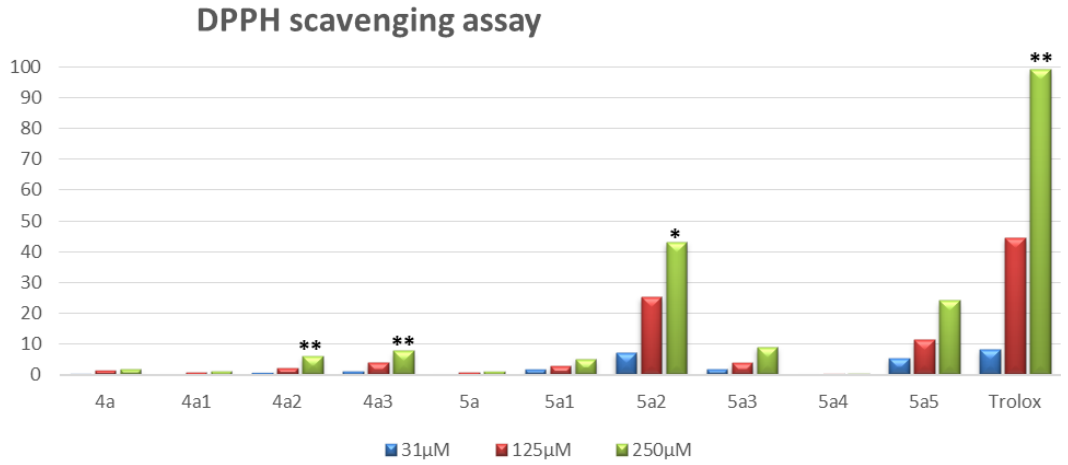

Figure 4.

DPPH Radical Scavenging Activity the compounds at concentrations 31 to 250 µM

Standard deviation (SD) (n = 3). Significant difference *vs*. control: *p < 0.01; **p < 0.001

The entries constructed out of valine-based acid (**4a1-4a3**) displayed insignificant DPPH scavenging activities. The former observation agreed with the results delivered from the ABTS$^{+\bullet}$ experiments. Compounds **5a2** and **5a5** discoloured the DPPH solution, thus moderate antioxidant capacities were detected. However, the latter compounds showed lower DPPH scavenging activities when compared to Trolox.

Analysing the data from both antioxidant bioassays, some common characteristics could be observed. The amide based compound **5a2** revealed the most prominent antioxidant capacity when the DPPH and the ABTS$^{+\bullet}$ scavenging assays were considered. Therefore, the piperazine moiety could be examined as a potent scaffold for a future design of novel antioxidants. The latter results are in good agreement with recent papers which have discussed good radical scavenging

activities of numerous substituted piperazines [17, 29, 31]. Interestingly, the valine-based pyrrole derivatives did not demonstrate any antioxidant properties after both assays. However, it should be noted that the amide substituents are dissimilar to those applied in the second series of compounds. Therefore, further examinations should be conducted.

MAO-B inhibitory activity assay

Both 1H-Pyrrole-1-yl acids (**4a** and **5a**) showed 10% MAO-B blocking capacities, as compared to selegiline (Figure 5). Out of all investigated structures, **5a2** demonstrated the most prominent MAO-B inhibitory activity – 20% at 1 μM concentration. Insignificant inhibitions were observed when examining **5a1** – 7%, **5a3** – 3%, **5a4** – 7% and **5a5** - 9%. Interestingly, all compounds included in the first class (except **4a**) induced the MAO-B activity. The enzyme induction capacity was as follows: **4a3** – 63%, **4a1** – 44% and **4a2** – 24%.

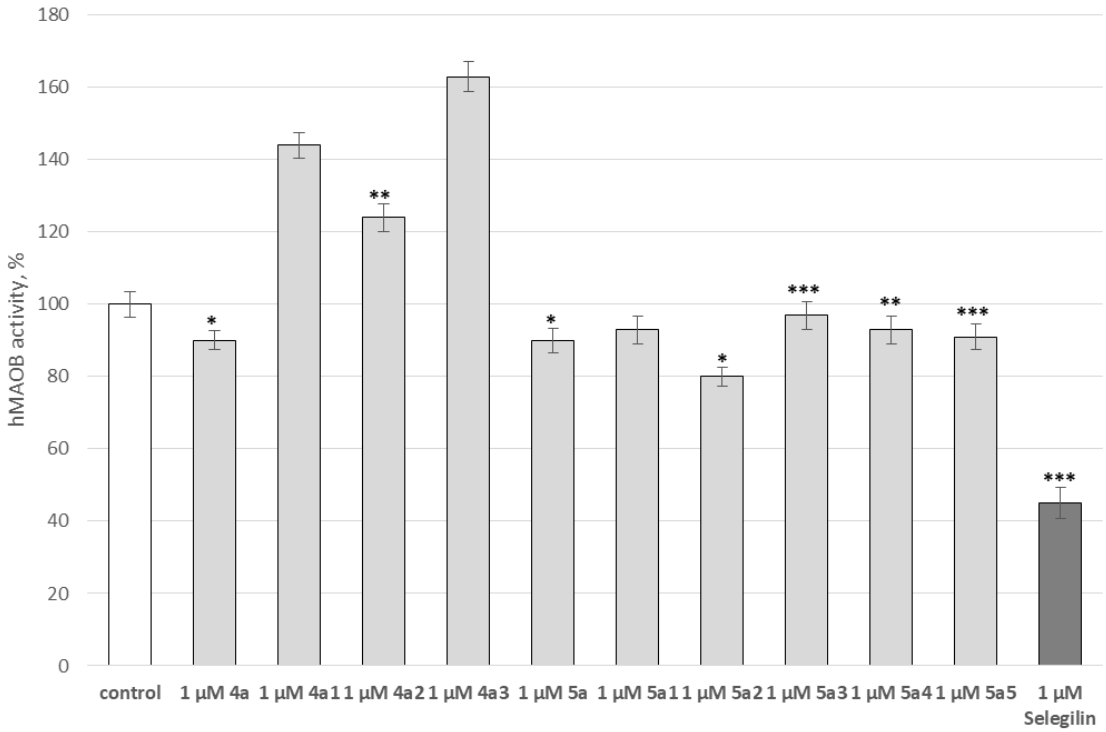

Figure 5.

Effects of the pyrrole acids and the amide derivatives (at concentration 1 μM), on hMAOB

* $p < 0.05$; ** $p < 0.01$; *** $p < 0.001$ *vs.* control (pure hMAOB)

When comparing the MAO-B activities of the aforementioned structures, we found the promising role of 1-(4-bromophenyl)piperazine in the blocking process of the latter enzyme. Moreover, when we altered the coupling amine to 1-(4-chlorobenzyl)piperazine moiety, the MAO-B antagonizing capacity dropped drastically – from 20% to 7%. Comparing the two applied series of compounds – **4a, 4a1-4a3** and **5a, 5a1-5a5**, we indicated that the presence of a valine pyrrole-based amides, led to an opposing effect of MAO-B inducement.

Overall, the examined MAO-B effects of the structures demonstrated that the latter could be applied for further optimization in the process of finding new and effective pyrrole-based MAO-B inhibitors.

Molecular docking studies

In order to observe the MAO-B effects of the pyrrole-based compounds and to identify the possible conformations, molecular docking simulations were carried out in the active site of MAO-B.

Compound **5a2,** which demonstrated the most prominent activity was applied in the docking simulations. Considering the lack of resolved crystallographic MAO-B receptors with chemically similar to our database co-crystallized ligands, we utilized the enzyme with PDB code - **6FW0**. The correlations between the *in silico* and *in vitro* results were in good agreement.

5a2 interacted with the active site of MAO-B through a variety of intermolecular interactions such as, hydrogen bonds, hydrophobic and π-π interactions (Figure 6). The 1-(4-bromophenyl)piperazine moiety was in close vicinity to the flavin adenine dinucleotide (FAD) of MAO-B and demonstrated strong π-π stacking interactions with residues Tyr435 and Tyr398. The latter amino acids are the key factor in the formation of a stable ligand-MAO-B complex [15]. Due to the position of the Br atom and its strong halogen bond donating ability, a halogen bond between the former and FAD was observed. The distance of the bond was calculated to be 4.99 Å. The Ile199 residue was

heavily involved in the formation of stable complex. The latter participated in P-alkyl interactions with the piperazine, pyrrole and p-bromophenyl substituent in the pyrrole ring. Hydrogen bond with Tyr326 was also observed, which could be accounted for higher selectivity towards MAO-B, as MAO-A comprises Ile335 residue instead of Tyr326 [15]. The distance of the conventional hydrogen bond was noted to be 2.43 Å. In addition, favourable interactions were created with Leu167, Ile316, Leu88, Glu84, Pro104, Leu164 and Ile198 active amino residues.

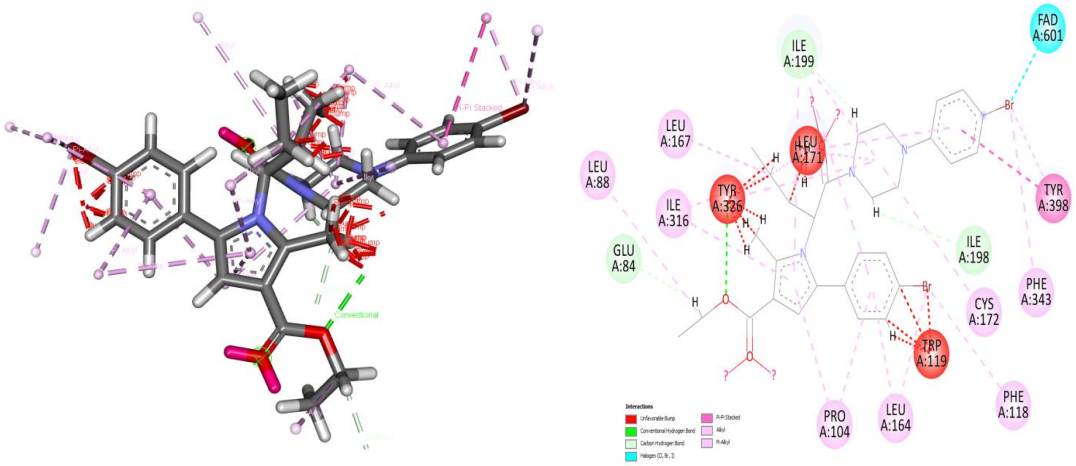

Figure 6.
Docking of the most active MAO-B inhibitor (2A2) represented in 3D and 2D forms, respectively

Interestingly, several unfavourable interactions between **5a2** and the active site of MAO-B were observed, which unambiguously leads to a drastic lowering of the MAO-B blocking capacity. A steric clash between the 4-bromophenyl moiety in the pyrrole ring and Trp119 residue was detected. Furthermore, the side chain of the Isoleucine amino acid utilized for the condensation reaction, participated in two unfavourable bumps with Tyr326 and Leu171 amino residues.

With the former examination it could be clearly stated that applying small, non-branched amino acids or carboxylic acids with terminal primary amine groups for the Paal-Knorr condensation, would feasibly introduce more potent MAO-B inhibitors. Moreover, removing the bulky p-bromophenyl group located at fifth position in the pyrrole moiety could result in more potent inhibitors.

ADME

As a final step, we conducted an *in silico* ADME analysis to examine the pharmaceutically relevant properties of the most prominent compounds in our dataset. The QikProp module in Maestro 11.8 was utilized for the determination of the absorption, distribution, metabolism and excretion (ADME) of the compounds. Considering the obtained results, we concluded that compounds **4a** and **5a** have excellent physicochemical properties related to 95% of the existing drugs, while the most active antioxidant and MAO-B inhibitor in both series – **5a2,** exerted a moderate range of drug-like properties. Two of the calculated descriptors – QPlogP and QPlogS, felt out of range during the conducted simulations. Values of 6.997 and -8.471, respectively, were observed. However, the determined brain/blood partition coefficient (QPlogBB) of all examined compounds was in the optimal range of –3.0 – 1.2, which is mandatory for potential MAO-B inhibitors [20].

Conclusions

Two series of pyrrole-based amides with isoleucine and valine linkers were designed, synthesized and evaluated for their antioxidant and MAO-B capacities. All of the tested compounds showed variable MAO-B blocking activities. Both free radical scavenging bioassays – DPPH and $ABTS^{+\bullet}$, demonstrated that compounds with piperazine moieties exerted good to excellent antioxidant properties. In particular, compound **5a2** was found to be the most prominent derivative as it displayed great antioxidant and MAO-B blocking effects. After the molecular docking simulations, we suggested that reducing the substituents in the pyrrole ring could greatly enhance the MAO-B blocking properties. Moreover, the ADME tests showed that the compounds possess good to excellent physico-chemical properties and the latter could be applied in future optimizations.

Acknowledgement

This study was supported and financed by Contract №100/04.06.2021, Project №7901/19.11.2020 of the Council of Medical Sciences, Medical University – Sofia.

Conflict of interest

The authors declare no conflict of interest.

References

1. Arnao MB, Cano A, Acosta M, The hydrophilic and lipophilic contribution to total antioxidant activity. *Food Chem.*, 2001; 73(2): 239-244.
2. Bautista-Aguilera OM, Esteban G, Bolea I, Nikolic K, Agbaba D, Moraleda I, Iriepa I, Samadi A, Soriano E, Unzeta M, Marco-Contelles J, Design, synthesis, pharmacological evaluation, QSAR analysis, molecular modeling and ADMET of novel donepezil–indolyl hybrids as multipotent cholinesterase/monoamine oxidase inhibitors for the potential treatment of Alzheimer's disease. *Eur J Med Chem.*, 2014; 75: 82-95.
3. Bhabak KP, Mugesh G, Functional mimics of glutathione peroxidase: bioinspired synthetic antioxidants. *Acc Chem Res.*, 2010; 43(11): 1408-1419.
4. Bijev A, Nankov A, Prodanova P, Synthesis of N-pyrrolylacetic and 3-(N-pyrrolyl)propanoic acids. *Compt Rend Acad Bulg Sci.*, 2000; 53: 29-32.
5. Brand-Williams W, Cuvelier ME, Berset C, Use of a free radical method to evaluate antioxidant activity. *LWT - Food Sci Technol.*, 1995; 28(1): 25-30.
6. Butterfield DA, Halliwell B, Oxidative stress, dysfunctional glucose metabolism and Alzheimer disease. *Nat Rev Neurosci.*, 2019; 20(3): 148-160.
7. Cho HU, Kim S, Sim J, Yang S, An H, Nam MH, Jang DP, Lee CJ, Redefining differential roles of MAO-A in dopamine degradation and MAO-B in tonic GABA synthesis. *Exp Mol Med.*, 2021; 53(7): 1148-1158.
8. Elkamhawy A, Paik S, Park JH, Kim HJ, Hassan AHE, Lee K, Park KD, Roh EJ, Discovery of novel and potent safinamide-based derivatives as highly selective hMAO-B inhibitors for treatment of Parkinson's disease (PD): Design, synthesis, *in vitro*, *in vivo* and *in silico* biological studies. *Bioorg Chem.*, 2021; 115: 105233: 1-14.
9. Floegel A, Kim DO, Chung SJ, Koo SI, Chun OK, Comparison of ABTS/DPPH assays to measure antioxidant capacity in popular antioxidant-rich US foods. *J Food Compost Anal.*, 2011; 24(7): 1043-1048.
10. Knopman DS, Jones DT, Greicius MD, Failure to demonstrate efficacy of aducanumab: An analysis of the EMERGE and ENGAGE trials as reported by Biogen, December 2019. *Alzheimers Dement.*, 2021; 17(4): 696-701.
11. Lipinski CA, Lombardo F, Dominy BW, Feeney PJ, Experimental and computational approaches to estimate solubility and permeability in drug discovery and development settings. *Adv Drug Deliv Rev.*, 2001; 46(1-3): 3-26.
12. Madhavi Sastry G, Adzhigirey M, Day T, Annabhimoju R, Sherman W, Protein and ligand preparation: parameters, protocols, and influence on virtual screening enrichments. *J Comput Aided Mol Des.*, 2013; 27(3): 221-234.
13. Maramai S, Benchekroun M, Gabr MT, Yahiaoui S, Multitarget Therapeutic Strategies for Alzheimer's Disease: Review on Emerging Target Combinations. *Biomed Res Int.*, 2020; 2020: 5120230: 1-27.
14. Matthews KA, Xu W, Gaglioti AH, Holt JB, Croft JB, Mack D, McGuire LC, Racial and ethnic estimates of Alzheimer's disease and related dementias in the United States (2015-2060) in adults aged ≥65 years. *Alzheimers Dement.*, 2019; 15(1): 17-24.
15. Milczek EM, Binda C, Rovida S, Mattevi A, Edmondson DE, The 'gating' residues Ile199 and Tyr326 in human monoamine oxidase B function in substrate and inhibitor recognition. *FEBS J.*, 2011; 278(24): 4860-4869.
16. Abid SM, Younus, HA, Al-Rashida M, Arshad Z, Maryum T, Gilani MA, Alharthi AI, Iqbal J, Sulfonyl hydrazones derived from 3-formylchromone as non-selective inhibitors of MAO-A and MAO-B: Synthesis, molecular modelling and *in-silico* ADME evaluation. *Bioorg Chem.*, 2017; 75: 291-302.
17. Patel RV, Mistry B, Syed R, Rathi AK, Lee YJ, Sung JS, Shinf HS, Keum YS, Chrysin-piperazine conjugates as antioxidant and anticancer agents. *Eur J Pharm Sci.*, 2016; 88: 166-177.
18. Pérez-Areales FJ, Betari N, Viayna A, Pont C, Espargaró A, Bartolini M, De Simone A, Rinaldi Alvarenga JF, Pérez B, Sabate R, Lamuela-Raventós RM, Andrisano V, Luque FJ, Torrero DM, Design, synthesis and multitarget biological profiling of second-generation anti-Alzheimer rhein–huprine hybrids. *Future Med Chem.*, 2017; 9(10): 965-981.
19. Pohanka M, Oxidative stress in Alzheimer disease as a target for therapy. *Bratisl Lek Listy.*, 2018; 119(9): 535-543.
20. Poovaiah N, Davoudi Z, Peng H, Schlichtmann B, Mallapragada S, Narasimhan B, Wang Q, Treatment of neurodegenerative disorders through the blood–brain barrier using nanocarriers. *Nanoscale*, 2018; 10(36): 16962-16983.
21. Prashanth MK, Revanasiddappa HD, Lokanatha Rai KM, Veeresh B, Synthesis, characterization, antidepressant and antioxidant activity of novel piperamides bearing piperidine and piperazine analogues. *Bioorg Med Chem Lett.*, 2012; 22(23): 7065-7070.
22. Rajan P, Vedernikova I, Cos P, Berghe DV, Augustyns K, Haemers A, Synthesis and evaluation of caffeic acid amides as antioxidants. *Bioorg Med Chem Lett.*, 2001; 11(2): 215-217.
23. Sano M, Ernesto C, Thomas RG, Klauber MR, Schafer K, Grundman M, Woodbury P, Growdon J, Cotman CW, Pfeiffer E, Schneider LS, Thal LJ, A controlled trial of selegiline, alpha-tocopherol, or both as treatment for Alzheimer's disease. The Alzheimer's Disease Cooperative Study. *N Engl J Med.*, 1997; 336(17): 1216-1222.
24. Schedin-Weiss S, Inoue M, Hromadkova L, Teranishi Y, Yamamoto NG, Wiehager B, Bogdanovic N, Winblad B, Sandebring-Matton A, Frykman S, Tjemberg LO, Monoamine oxidase B is elevated in Alzheimer disease neurons, is associated with γ-secretase and regulates neuronal amyloid β-peptide levels. *Alzheimers Res Ther.*, 2017; 9(1): 57-64.
25. Smith MA, Perry G. The Role of Oxidative Stress in the Pathological Sequelae of Alzheimer Disease. Free Radicals, Oxidative Stress, and Antioxidants: Springer US; 1998; 195-204.
26. Szökő É, Tábi T, Riederer P, Vécsei L, Magyar K, Pharmacological aspects of the neuroprotective effects of irreversible MAO-B inhibitors, selegiline

and rasagiline, in Parkinson's disease. *J Neural Transm (Vienna)*, 2018; 125(11): 1735-1749.
27. Stankova I, Lazarova M, Chayrov R, Popatanasov A, Tancheva L, Kalfin R, Newly synthesized amantadine derivative: safety and neuropharmacological activity. *Farmacia*, 2021; 69(6): 1112-1119.
28. Türkeş C, Investigation of Potential Paraoxonase-I Inhibitors by Kinetic and Molecular Docking Studies: Chemotherapeutic Drugs. *Protein Pept Lett.*, 2019; 26(6): 392-402.
29. Valachová K, Mach M, Šoltés L, Oxidative Degradation of High-Molar-Mass Hyaluronan: Effects of Some Indole Derivatives to Hyaluronan Decay. *Int J Mol Sci.*, 2020; 21(16): 5609: 1-12.
30. Vladimirova S, Bijev A, An access to new N-pyrrolylcarboxylic acids as potential COX-2 inhibitors *via* Paal-Knorr cyclization. *Heterocycl Commun.*, 2014; 20(2): 111-115.
31. Zhang RH, Guo HY, Deng H, Li J, Quan ZS, Piperazine skeleton in the structural modification of natural products: a review. *J Enzyme Inhib Med Chem.*, 2021; 36(1): 1165-1197.
32. Zhou S, Chen G, Huang G, Design, synthesis and biological evaluation of lazabemide derivatives as inhibitors of monoamine oxidase. *Bioorg Med Chem.*, 2018; 26(17): 4863-4870.
33. *** www.rcsb.org.